

HPCMP CREATE™-AV Kestrel Simulations for the DPW-8/AePW-4 Buffet Working Group: Part 1

Steven E. Lamberson, Jr.*

Bowhead Total Enterprise Solutions LLC, Springfield, VA 22150

Brent W. Pomeroy† and Tausif Jamal‡

NASA Langley Research Center, Hampton, VA 23681

This paper documents some computational explorations performed for the Buffet Working Group of the combined eighth AIAA Drag Prediction Workshop and the fourth Aeroelastic Prediction Workshop. The computational explorations were performed using HPCMP CREATE™-AV Kestrel as part of a collaborative effort between the Kestrel development team and some Kestrel users in the NASA Langley Research Center Configuration Aerodynamics Branch. The test case in question is a two-dimensional airfoil at Mach 0.73 at ten angles of attack between 1.36° and 3.90°, including various angles of attack that demonstrated buffeting behavior in the experiments. The simulations make use of the Spalart-Allmaras (SA) and Menter Shear Stress Transport (SST) turbulence models run in both steady and unsteady modes to compare to mean pressure and RMS pressure distributions measured experimentally. For the angles of attack pre-buffet, simulations using both turbulence models show fairly good agreement with the experimental data. For the angles of attack post-buffet, simulations using the SST turbulence model capture the trends in the data well, while the simulations using the SA turbulence model fail to demonstrate significant unsteady behavior.

I. Introduction

High-speed buffet, an adverse aerodynamic phenomenon that occurs at the edge of the flight envelope, is the topic of study for the Buffet Working Group of the upcoming multidisciplinary Drag Prediction Workshop 8/Aeroelastic Prediction Workshop 4 (DPW-8/AePW-4) [1–3].

Transport aircraft can be subjected to buffet at a range of conditions, most notably at Mach numbers (M) and lift coefficient (C_L) that exceed the nominal mid-cruise condition. It is an undesirable condition in which aerodynamic unsteadiness can threaten the structural integrity of the vehicle and stress fly-by-wire control laws. If M and/or C_L is even higher than buffet, flutter can be experienced, which is the coupling of unsteady aerodynamic features and the structural modes. Flutter can lead to catastrophic vehicle loss [4]. Consequently, a multidisciplinary approach must be considered at these extreme conditions, which has led to the collaborative DPW-8/AePW-4, planned for the summer of 2026.

Swept-wing vehicles may experience pitch-up when the flow over the mid-span or outboard portion of the wing separates. As this region of the wing is downstream of the center of gravity, a nose-up pitching moment (C_M) is observed. Without proper control, the nose-up C_M will cause the angle of attack (α) to increase, leading the vehicle deeper into the stall regime. With high enough α , the separated wing wake may impinge upon the horizontal tail and cause massive stall, potentially leading to a total hull loss. Pitch-up, a significant focus in DPW-VII, occurs when the C_M - α curve is no longer linear and a decreased magnitude of C_M is observed with increasing α . A significant amount of scatter was observed post-pitch-up for the submissions, regardless of turbulence model, temporal scheme, discretization, and solver settings. Consequently, this regime became the subject of further investigation in DPW-8/AePW-4.

The Buffet Working Group will be exploring the buffet and pitch-up phenomena using three test cases. The first test case explores the phenomena in two dimensions using a static, transonic airfoil designed by the Office National d'Études et de Recherches Aérospatiales (ONERA). The second test case expands the exploration into three dimensions by looking at unsteady flow on the National Aeronautics and Space Administration (NASA) common research model

*HITS-R2 / CREATE-AV Kestrel Principal Developer; AIAA Senior Member.

†Aerodynamics Research Engineer, Configuration Aerodynamics Branch; AIAA Senior Member

‡Research Aerospace Engineer, Configuration Aerodynamics Branch; AIAA Member.

(CRM) wing-body-tail configuration using a static mesh. The third test case expands even further by adding aeroelastic deformation to the second test case.

This paper presents results for the first test case obtained as part of an inter-agency effort between the Department of Defense (DOD) High-Performance Computing Modernization Program (HPCMP) Computational Research and Engineering Acquisition Tools and Environments Air Vehicles (CREATE-AV) group and the NASA Langley Research Center Configuration Aerodynamics Branch. The data were generated in support of DPW-8/AePW-4 Mini Workshop 1, held at the 2025 American Institute of Aeronautics and Astronautics (AIAA) SciTech Forum and Exposition, and the Buffet Working Group Mini Workshop 2, held virtually in May 2025.

II. Test Case

The first test case for the Buffet Working Group makes use of the ONERA OAT15A transonic airfoil. This geometry has been the subject of extensive experimental and computational studies, including the reference experiment for this test case [5]. The experiment ran an α sweep at Mach 0.73, $Re_c = 3 \times 10^6$, and a static freestream temperature of 271 K. The experiment found that buffet onset, the α at which significant unsteadiness occurs, occurred around $\alpha \approx 3.1^\circ$. Data for the chord-wise pressure coefficient (C_P), the root-mean-square (RMS) of the chord-wise C_P , and pressure spectra extracted from the upper surface at the 40% chord location, are available for α of 2.50° , 3.00° , 3.10° , 3.25° , 3.50° , and 3.90° .

For the workshop, this test case was split into two segments. Test case 1a was to look at all α for which experimental data is available, as well as 1.36° , 1.50° , 3.40° , and 3.60° , using steady analysis and multiple mesh densities. Test case 1b was to look at all the same α as test case 1a, but focusing on unsteady analysis using a medium-density grid.

A. Grid

The DPW-8/AePW-4 organizing committee provided standard grids for participants and encouraged the use of these grids to maintain consistency between submissions [6–8].* This study used the Cadence unstructured mixed-element six-member grid family, which was generated in compliance with the committee-specified gridding guidelines. The target grid density is the medium-density grid. Density was coarsened and refined from that point to generate a family including L1 (“tiny”), L2 (“coarse”), L3 (“medium”), L4 (“fine”), L5 (“extra fine”), and L6 (“ultra fine”), and key metrics are tabulated in Table 1. The right-most column in the table represents the target y^+ , a nondimensional first-cell height grid metric. While y^+ is dependent upon the flow field, target values are specified near the cruise point.

Table 1 Cadence Unstructured Grid Metrics

Grid Level	Number of Cells	Target y^+
1	47,187	1.00
2	89,616	0.67
3	150,333	0.50
4	235,491	0.40
5	353,725	0.33
6	517,448	0.29

Figure 1 shows the region close to the airfoil for the entire grid family. As seen, a progressive refinement of the grids was applied with topologically similar grid densities over the airfoil surface.

III. Method Description

The simulations discussed in this paper make use of version 12.10 of the HPCMP CREATE™-AV Kestrel software package [9]. Kestrel’s focus is robust and accurate performance predictions of fixed-wing air vehicles relevant to the U.S. DOD, and incorporates steady and unsteady aerodynamics, thermochemistry, structural dynamics, conjugate heat

*https://dpw.larc.nasa.gov/DPW8/ONERA_OAT15A/, last accessed on 2025-06-02.

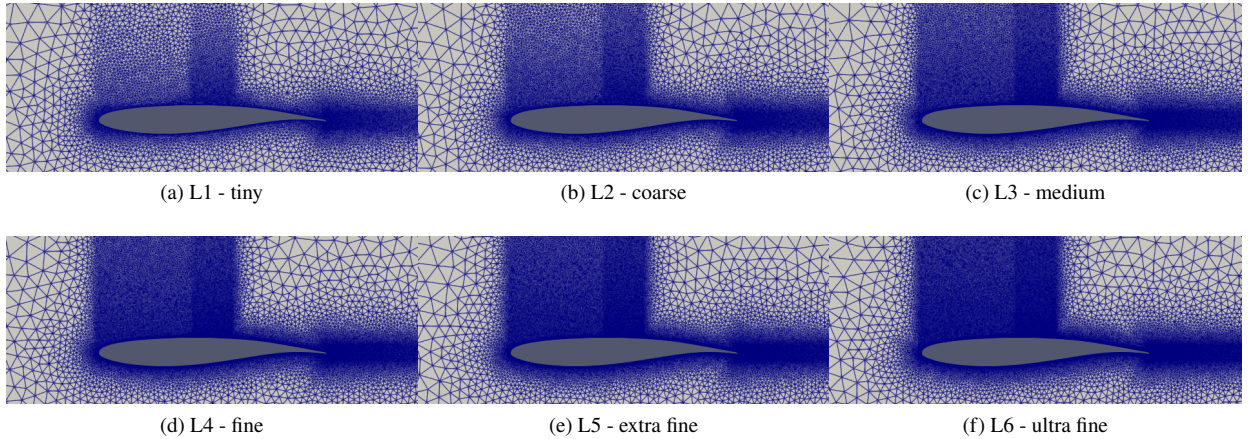


Fig. 1 Region near airfoil for all grids in the Cadence unstructured grid family.

transfer, stability and control, propulsion, and more. While the simulations discussed in this paper only make use of Kestrel’s aerodynamic simulation capabilities, future problems considered by Buffet Working Group will use Kestrel’s multi-physics simulation capabilities combining unsteady aerodynamics with structural dynamics.

The present work makes use of KCFD, which is Kestrel’s second-order, cell-centered, finite-volume unstructured fluid dynamics solver. KCFD supports heterogeneous unstructured meshes consisting of triangles or quadrilaterals in 2D or tetrahedrons, prisms, pyramids, or hexahedrons in 3D. KCFD is capable of achieving up-to second-order accuracy in both space and time. For time-accurate simulations, second-order temporal accuracy is achieved by a subiterative scheme [10] with a second-order backward difference formula (BDF2). For steady simulations, the solver uses a single subiteration, a first-order backward difference formula (BDF1), and a different time-step for each cell computed from a user-specified Courant-Friedrichs-Lowy (CFL) number.

KCFD solves both the steady and unsteady forms of the Reynolds-averaged Navier-Stokes (RANS) equations using either the Spalart-Allmaras (SA) one-equation turbulence model or the Menter two-equation turbulence model [11]. The Menter model supports the “baseline” Menter model, the shear stress transport (SST) model, and a modified version of the SST model called “SSTM” [12]. Both models include an optional rotational/curvature (RC) correction as well as an optional quadratic constitutive relation (QCR) extension. Both models also support including delayed detached-eddy simulation (DDES) terms using either the improved DDES (iDDES) or Shear Layer Adapted (SLA) formulations. The present work compares the SA turbulence model to the SST turbulence model, both with the optional RC and QCR extensions enabled.

KCFD includes a flexible definition of its gradient stencils based on user input. The stencil can include any combination of the cells that share a face with the cell of interest (first-level face neighbors, or FN1), the cells that share a face with each cell that shares a face with the cell of interest (second-level face neighbors, or FN2), and cells which share a node with the cell of interest (node neighbors, or NN). By default, only the FN1 cells are included in the stencil. The present work explores solutions using the FN1+NN stencil.

KCFD supports a variety of options controlling the solver including different choices for inviscid flux schemes, viscous flux schemes, and limiters. The present work makes use of the HLLE++ inviscid flux scheme, the Alpha-Damping viscous flux scheme, and a Kestrel-specific limiter called “KestrelSmooth+”. The “KestrelSmooth+” limiter is an improved version of Kestrel’s default limiter, which is a continuous form of the Barth-Jesperson limiter.

IV. Results

Computational explorations were done on the ONERA OAT15A airfoil described in section II using the KCFD solver described in section III. Test case 1a was the steady exploration, and will be discussed in Section IV.A. Test case 1b was the unsteady exploration, and will be discussed in Section IV.B.

A. Steady Analysis

Simulations were done at all ten α for all six grid levels using KCFD's steady solver with a prescribed CFL number of 1000. Simulations were done for 50,000 iterations, which was sufficient for the solver residuals as well as the C_L , drag coefficient (C_D), and C_M to achieve their “steady” state. When an average value for C_L , C_D , or C_M is needed, the averages are computed starting at iteration 30,000 for each simulation. Recall that the flow seen in the experiment was unsteady starting at $\alpha \approx 3.1^\circ$, so solutions using a steady solver for these unsteady conditions are suspect.

Figure 2 shows how the lift progressed as a function of iteration for each of the α and each grid level for the SA turbulence model. For the lower α , all grid levels show steady convergence, and the solutions gather around the solution obtained on the finest mesh. Starting with $\alpha = 3.50^\circ$, the finest mesh starts to show significant oscillation that is representative of the steady solver trying to solve a flow that is actually unsteady. As α increases further, grid levels 4 and 5 also begin to exhibit this unsteady behavior. Grid levels 1-3 remain steady at all α .

Figure 3 shows how the lift progressed as a function of iteration for each of the α and each grid level for the SST turbulence model. For the lower α , all grid levels show steady convergence, and the converged solution is the same for all grid levels for a given α . Starting with $\alpha = 3.00^\circ$, the L6 mesh shows convergence indicative of the steady solver trying to solve an unsteady problem, and the L3 mesh exhibits difficulty damping out the unsteadiness, but all other mesh levels show steady behavior. As α increases beyond 3.00° , the other mesh levels start to show increased signs that the flow might not be steady, although for some reason the L3 mesh shows this increased unsteadiness the least.

Figure 4 shows the grid convergence for the mean values of C_L , C_D , and C_M when using the SA turbulence model, where the x -axis, $N^{-2/3}$, decreases as the number of cells in the grid (N) increases. The $\alpha = 3.10^\circ$ lines, around where buffet is first observed in the experiment, make use of the “square” symbol, while α below this use an upward-triangle and α above this use a downward-triangle. Typical grid convergence behavior, where the metric in question asymptotically approaches a value as $N^{-2/3}$ decreases, is seen for all $\alpha < 3.50^\circ$. For $\alpha = 3.50^\circ$ and above, the metrics start to diverge with the finer grids, and is most noticeable with the pitching-moment on the finest grid. Figure 5 shows the grid convergence for the SST turbulence model. Here, the desired grid convergence behavior is seen for angles of attack below $\alpha = 3.00^\circ$, and the finer grids show a more substantial deviation from the asymptotic behavior than was seen with the SA turbulence model.

Figure 6 shows how the lift varies as a function of α , drag, and pitching-moment for all the grid levels using the SA turbulence model. For mesh levels 1-3, the peak lift is observed at $\alpha = 3.40^\circ$, and all α above this see a decrease in lift, drag, and pitching-moment. For mesh levels 4-6, the lift, drag, and pitching-moment all continue to increase downstream of $\alpha = 3.40^\circ$. Figure 7 shows the same comparisons for all grid levels using the SST turbulence model. Here, only mesh levels 1-2 behave as expected. The L3 mesh starts to show increasing lift, drag, and pitching-moment starting at $\alpha = 3.50^\circ$. The α where this deviation starts decreases as the mesh level increases, with the finest mesh level showing the deviation starting at $\alpha = 3.00^\circ$.

The experimental measurements of the lift, drag, and pitching-moment are not known, so while the previous discussion is useful for distinguishing between the two turbulence models it is not possible to draw conclusions about which approach is closer to the experimental measurements. Figure 8 compares the mean pressure distribution around the airfoil for all the simulations to the mean pressure distributions measured in the experiments. For both turbulence models there is very little deviation between the grid levels, which is partially attributed to the use of the expanded “FN1+NN” gradient stencil. Only the SST simulations done with the L6 grid show deviations from the other SST computations, and these are only visible for $\alpha \geq 3.00^\circ$. For all α the location of the shock is slightly further downstream for the SA model than it is for the SST model. For lower α , the shock location obtained by SST is slightly upstream of the experimental measurements while the shock location obtained by SA is slightly downstream of the experimental measurements. For $\alpha = 2.50^\circ$ and $\alpha = 3.25^\circ$ the location of the shock found by SST is very close to the location measured in the experiments. For $\alpha = 3.50^\circ$ and $\alpha = 3.90^\circ$, the shock measured by the experiment is shallower than at the lower α , but the shocks found by both SA and SST remain steep at these α .

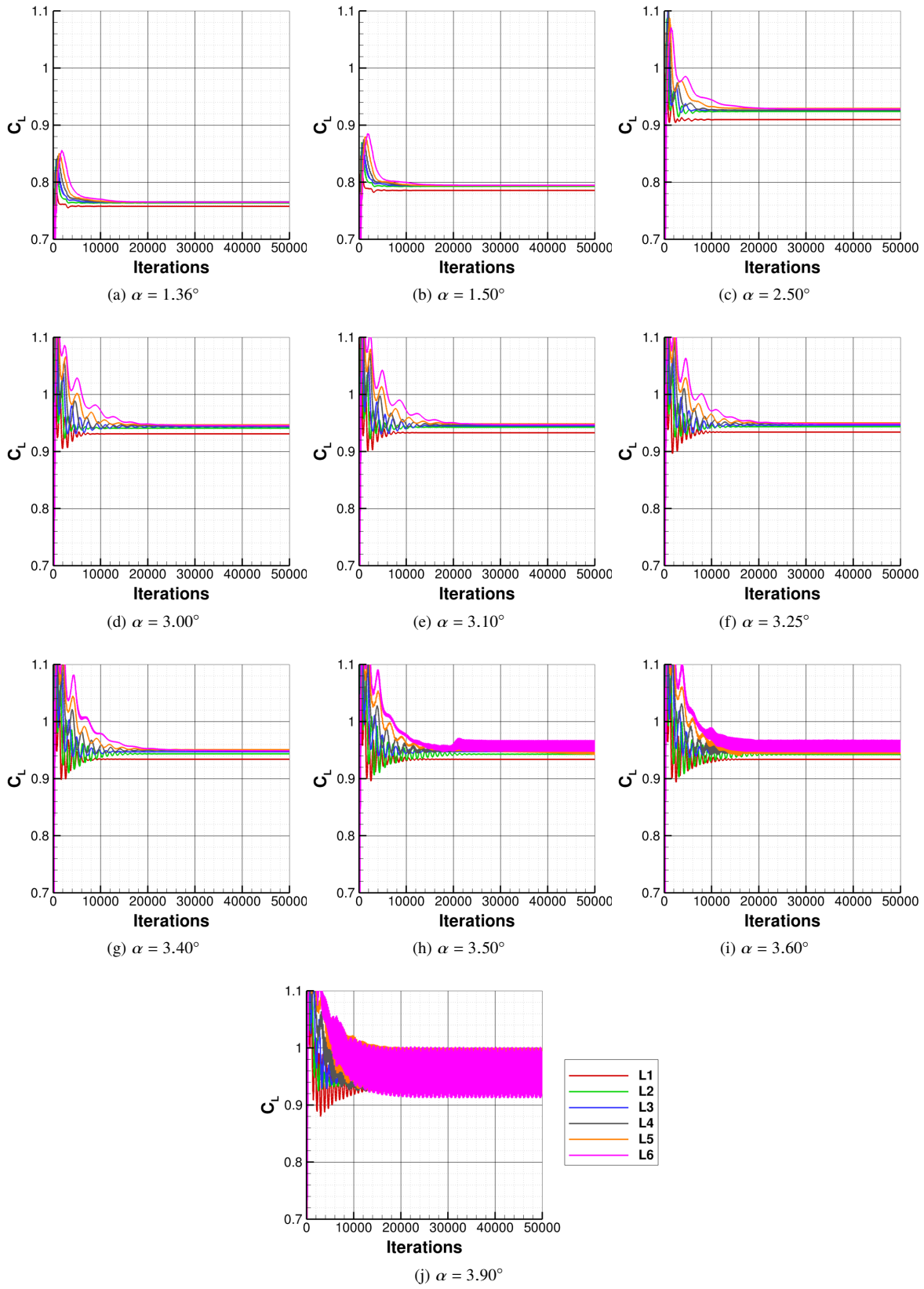


Fig. 2 Lift coefficient convergence history for the SA turbulence model.

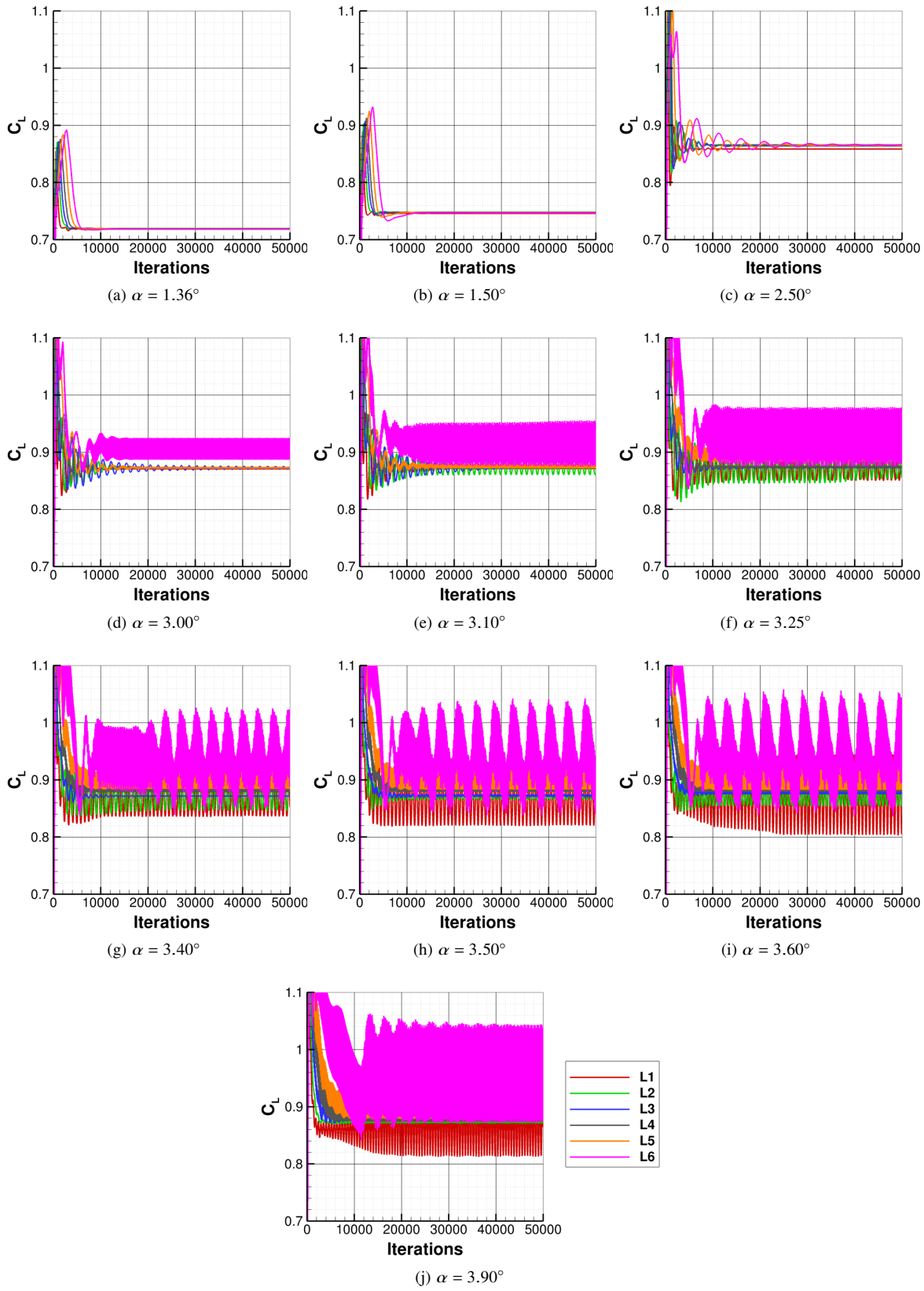


Fig. 3 Lift coefficient convergence history for the Menter SST turbulence model.

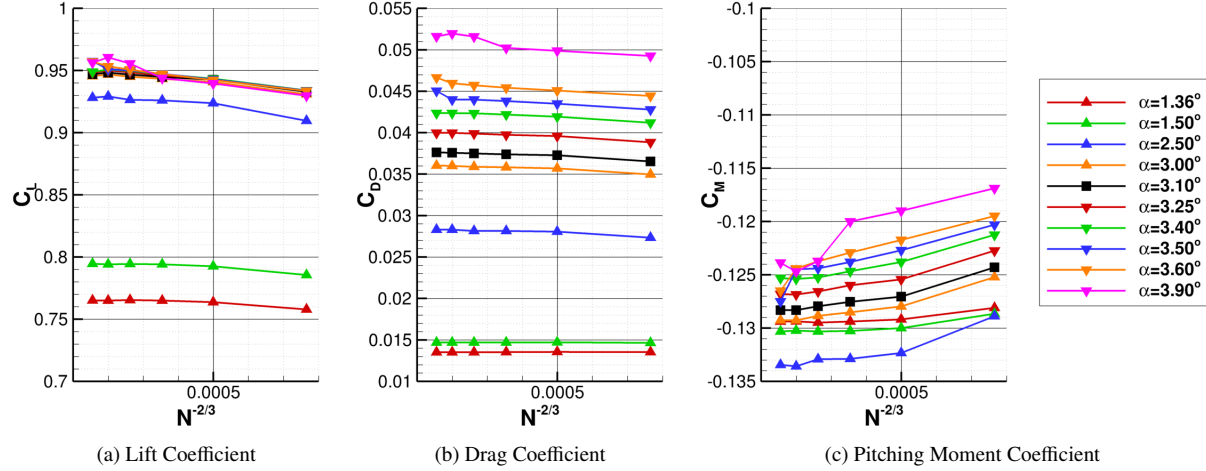


Fig. 4 Integrated loads grid convergence for the SA turbulence model.

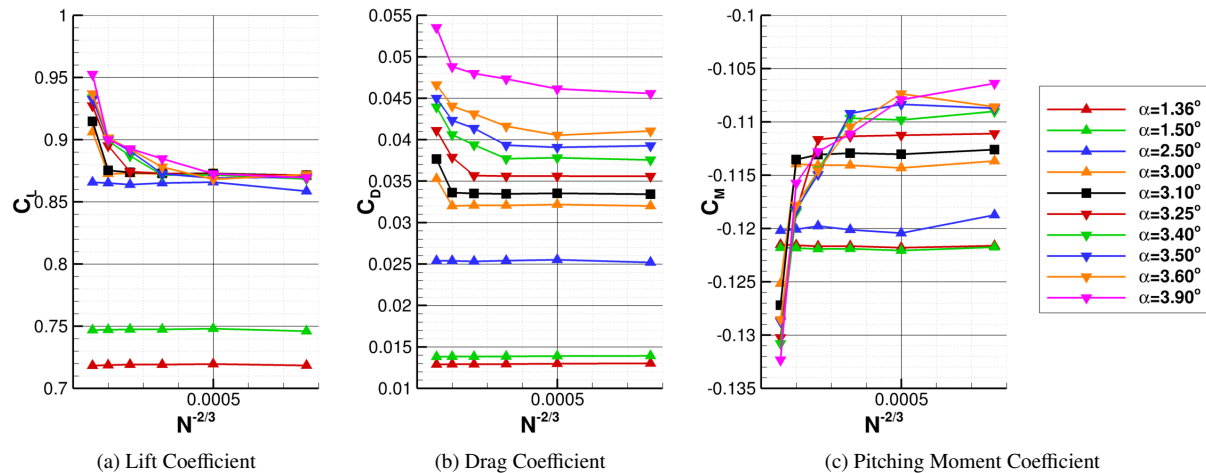


Fig. 5 Integrated loads grid convergence for the Menter SST turbulence model.

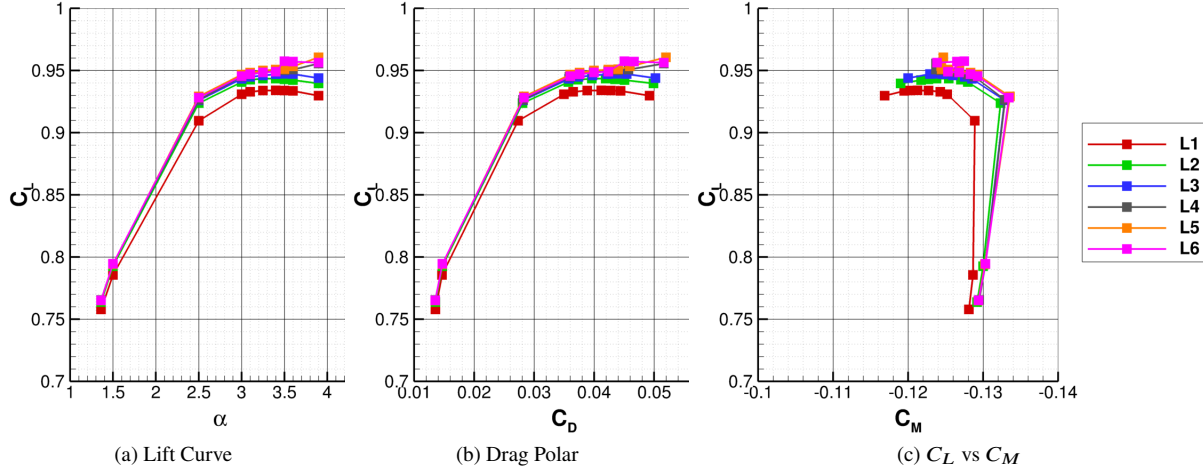


Fig. 6 Lift curve, drag polar, and C_L vs C_M plots for the SA turbulence model.

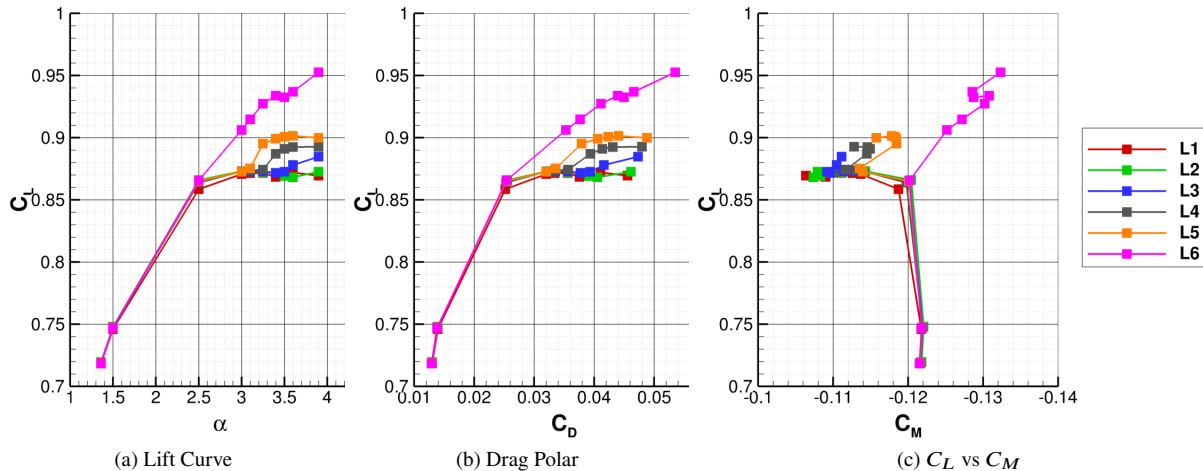


Fig. 7 Lift curve, drag polar, and C_L vs C_M plots for the SST turbulence model.

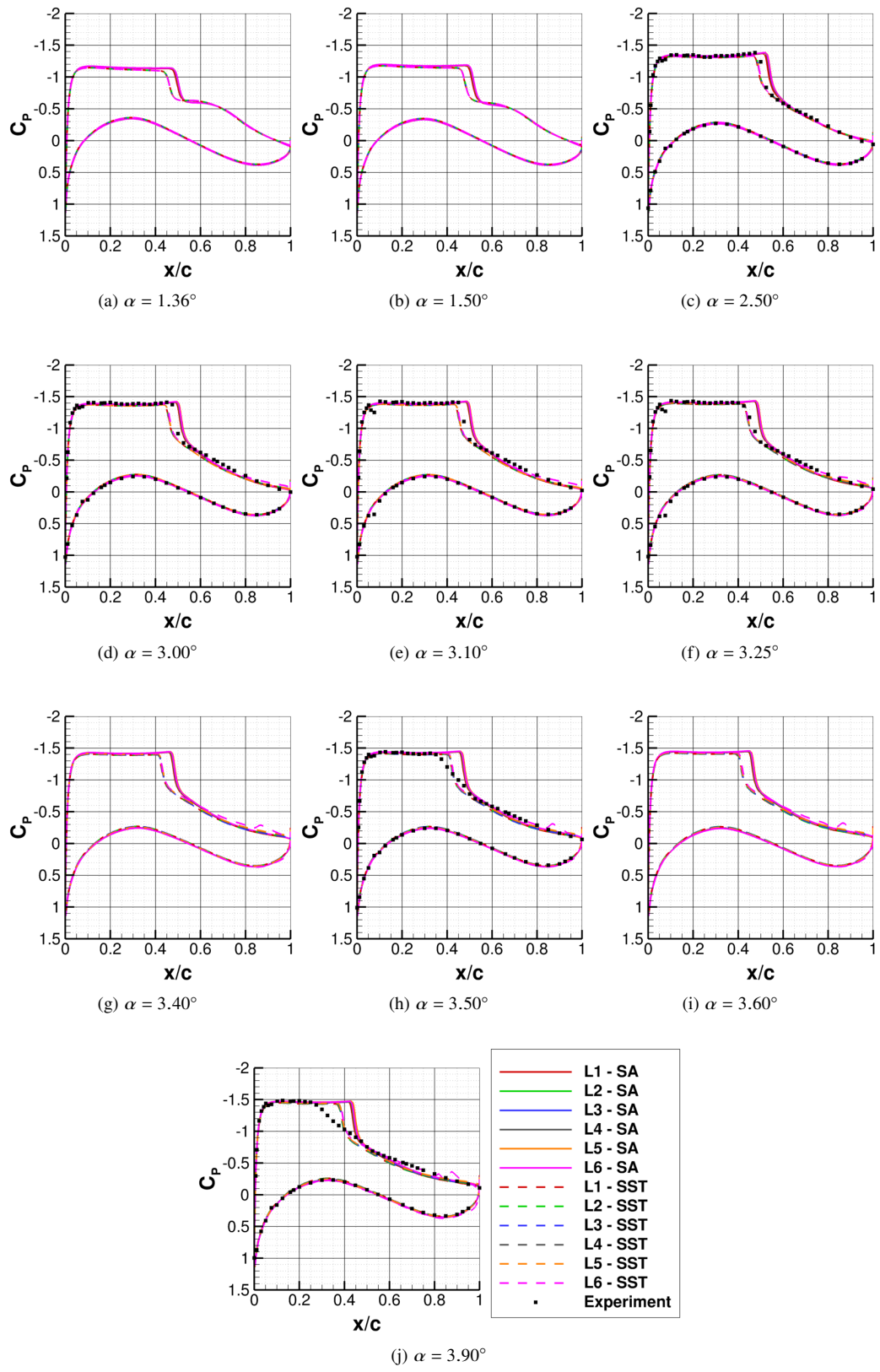


Fig. 8 C_P distribution.

B. Unsteady Analysis

For case 1b, the Buffet Working Group requested an unsteady analysis of all ten α , focusing on grid L3 if only one grid level is used. Unsteady analyses are sensitive to both the chosen time step and the number of subiterations used by the solver, so some explorations are needed before undertaking the entire α sweep. As a starting point, this exploration used the 3 subiterations recommended by the Kestrel documentation as a starting point and a time step of $\Delta t = CTU/200 = 0.005CTU$, where CTU is the critical time unit and is computed by dividing the reference length by the freestream velocity, or $CTU = L/U_\infty$. From there, subiterations are increased to 10 and the time step is decreased to $CTU/400$ and $CTU/800$.

Figure 9 shows how the C_L , C_D , and C_M vary with time for the various subiteration counts and time steps for the SA turbulence model at $\alpha = 3.90^\circ$ with grid L3. Decreasing the time step increases C_L and C_D while decreasing C_M . There is a significant jump in all three quantities between time steps, indicating the time step needs to be reduced further. There is no perceivable difference in the converged behavior between running a time step with 3 subiterations and running the time step with 10 subiterations. None of the simulations demonstrate noticeable unsteadiness, but this may change as smaller time steps are considered.

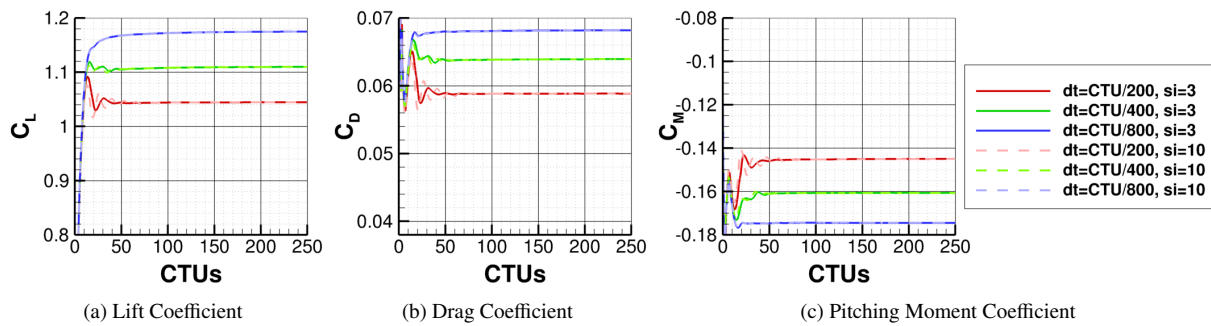


Fig. 9 Integrated loads convergence history for the SA turbulence model at $\alpha = 3.90^\circ$ using the L3 grid.

Figure 10 shows how the C_L , C_D , and C_M vary with time for the various subiteration counts and time steps for the SST turbulence model at $\alpha = 3.90^\circ$ with grid L3. When using 3 subiterations, all time steps converge to a steady solution and C_L and C_D increase while C_M decreases, indicating the time step needs to be reduced further. When using 10 subiterations, all time steps show significant unsteady behavior and it is difficult to tell from these plots how the various time steps differ from one another.

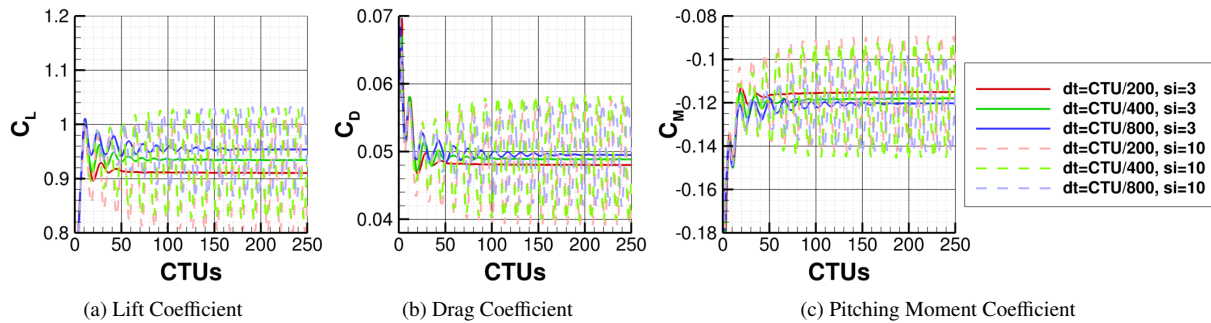


Fig. 10 Integrated loads convergence history for the SST turbulence model at $\alpha = 3.90^\circ$ using the L3 grid.

Figure 11 shows how the mean pressure distribution and the RMS of the pressure distribution varies with time step and subiteration count for both the SA and SST turbulence models. Looking at Figure 11a, the SA solutions show a shock location that is further downstream than the experimental measurements, and moves even further downstream as the time step decreases. The SST solutions using 3 subiterations show a shock location that is further downstream than the experimental measurements, but upstream of the SA shock locations. The SST solutions using 10 subiterations still

show a shock location that is further downstream than the experimental measurements and upstream of the SA shock locations, but the shape of the shock more closely matches the shape of the shock measured in the experiments.

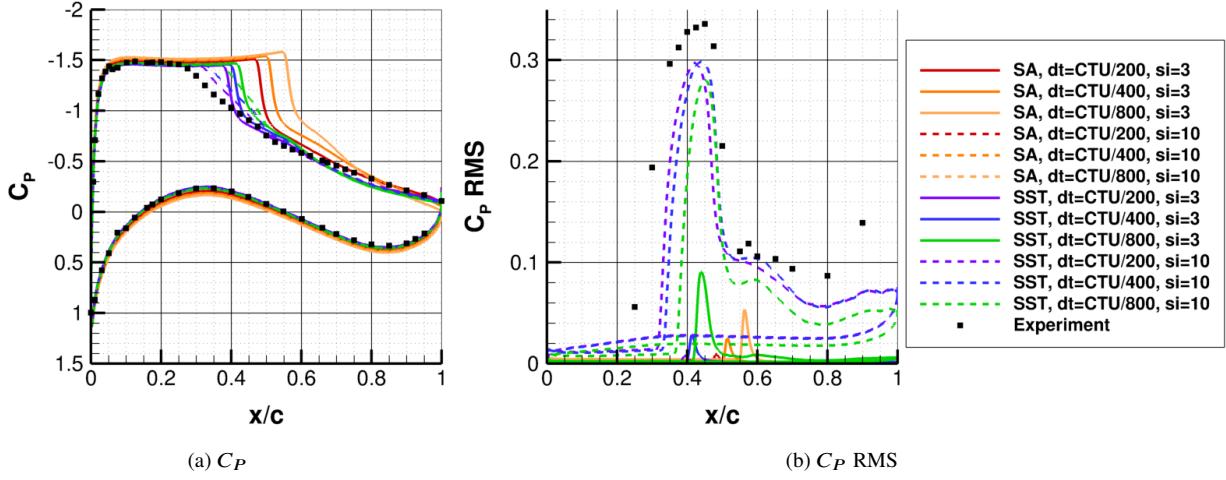


Fig. 11 Distribution of C_P and the C_P RMS at $\alpha = 3.90^\circ$ using the L3 grid.

Looking at Figure 11b, all the SA solutions and the SST solutions using 3 subiterations did not exhibit any significant unsteady behavior. The SST solutions using 10 subiterations show an RMS of the pressure distribution that is close to the experimental measurements in both shape and size. There are still noticeable differences in the unsteadiness as the time step decreases, even for the cases using 10 subiterations, indicating that a sufficiently small time step has not been achieved. In addition, preliminary analyses looking at the other α show very little unsteadiness even with 10 subiterations, further indicating that a smaller time step and/or more subiterations are needed at the lower α .

V. Future Work

The unsteady results discussed in Section IV.B indicate that further work is needed in order to complete the Buffet Working Group's test case 1b. Most importantly, further reduction in time step size and/or further increasing the number of subiterations used is needed to observe unsteady results for $\alpha < 3.90^\circ$. Furthermore, signs from Section IV.A indicate that the unsteadiness might be more pronounced on the finer grids, but the analysis in Section IV.B focused on only the L3 grid level.

VI. Conclusions

The ONERA OAT15A test case released as part of the Buffet Working Group of the combined 8th AIAA Drag Prediction Workshop and 4th AIAA Aeroelastic Prediction Workshop was simulated using HPCMP CREATE™-AV Kestrel simulation tool. The fluid solver KCFD was used for both steady-state RANS flow solutions as well as unsteady URANS flow solutions using both the SA turbulence model and the Menter SST turbulence model.

For the steady RANS runs, both the SA turbulence model and the SST turbulence model achieved reasonable results when compared to the mean pressure distribution measured by the experiment. The SA shocks tend to be slightly further downstream than the SST shocks, and for the lower α the experimental results tend to lie in between the SA and SST results. For larger α , the experimental shock moves further upstream than both the SA and SST results. The SST model simulations gave indications that the flow was probably unsteady starting at $\alpha = 3.00^\circ$, which is at a slightly lower α than where buffet onset was observed in the experiment. The SA model simulations largely failed to indicate that the flow might be unsteady, except for using the finest grids at the largest α .

The unsteady analyses completed thus far have focused on identifying an acceptable time step and number of subiterations, so the entire α sweep has not been conducted. For all time steps and subiteration counts explored at $\alpha = 3.90^\circ$ on the L3 mesh, the SA simulations did not exhibit notable unsteadiness. For all time steps explored at $\alpha = 3.90^\circ$ on the L3 mesh, the SST simulations done using 3 subiterations did not exhibit notable unsteadiness, however the SST simulations done using 10 subiterations showed an amount of unsteadiness in the ballpark of that observed in

the experiment. In addition, preliminary results using 10 subiterations for the other α did not show the expected amount of unsteadiness. Further work is needed to identify the correct time step and number of subiterations to use for both turbulence models that will work at all ten α .

Acknowledgments

Material presented here is a product of the Computational Research and Engineering for Acquisition Tools and Environments (CREATE) Program sponsored by the U.S. Department of Defense HPC Modernization Program (HPCMP) Office. Computations done in support of this effort were done on supercomputing resources provided by the HPCMP at the Navy DoD Supercomputing Resource Center (DSRC) and by the High-End Computing Capability (HECC) at the NASA Advanced Supercomputing (NAS) Facility.

The authors would like to thank Dr. Eric Lynch from the CREATE-AV Quality Assurance team for his advice.

References

- [1] Crouch, J., Garbaruk, A., Magidov, D., and Travin, A., "Origin and Structure of Transonic Buffet on Airfoils," AIAA Paper 2008-4233, 5th AIAA Theoretical Fluid Mechanics Conference, Seattle WA, 2008.
- [2] Crouch, J., Garbaruk, A., and Strelets, M., "Global Instability Analysis of Unswept- and Swept-Wing Transonic Buffet Onset," AIAA Paper 2018-3229, AIAA Fluid Dynamics Conference, Atlanta, GA, 2018.
- [3] Sansica, A., Pomeroy, B. W., Stanford, B. K., Ben-Gida, H., and Raveh, D. E., "DPW-8/AePW-4 Buffet Working Group: An Overview of Mini Workshops 1 and 2," To be presented at AIAA AVIATION Forum 2025.
- [4] Chwalowski, P., "AePW-4 High-Angle Working Group: An Overview of Recent Progress and Future Directions," To be presented at AIAA AVIATION Forum 2025.
- [5] Jacquin, L., Molton, P., Deck, S., Maury, B., and Soulevant, D., "Experimental Study of Shock Oscillation over a Transonic Supercritical Profiles," *AIAA Journal*, Vol. 47, No. 9, 2009, pp. 1985–1994.
- [6] Rider, B., and Pomeroy, B., "DPW-8 & AePW-4 Gridding Guidelines," https://aiaa-dpw.larc.nasa.gov/ref/gridding_guidelines_v3_07012024.pdf, 2024.
- [7] Pita, C. M., "DPW-8: ONERA OAT15A Meshes (Test Case 1)," 2024.
- [8] Hooker, R., and Wick, A., "DPW-8/AePW-4 Buffet Working Group: ONERA OAT15A 2-D Mesh Overview," 2024.
- [9] McDaniel, D. R., "A Summary of New and Emerging Features in HPCMP CREATE™ -AV Kestrel," *AIAA Scitech 2021 Forum*, AIAA, 2021. <https://doi.org/10.2514/6.2021-0234>.
- [10] Tomaro, R., Strang, W., and Sankar, L. N., "An Implicit Algorithm for Solving Time Dependent Flows on Unstructured Grids," *35th Aerospace Sciences Meeting and Exhibit*, 1997.
- [11] Nichols, R. H., "A Summary of the Turbulence Models in the CREATE-AV Kestrel Flow Solvers," *AIAA Scitech 2019 Forum*, AIAA, 2019. <https://doi.org/10.2514/6.2019-1342>.
- [12] Nichols, R. H., "Modification of the Turbulence Models in the CREATE™ -AV Kestrel Flow Solvers for High Speed Flows," *AIAA Scitech 2022 Forum*, AIAA, 2022. <https://doi.org/10.2514/6.2022-1174>.